Journal of Visualization, Vol. 11, No. 2 (2008)133-141

Regular Paper

Detached Shock Waves around Cylinders Flying at Mach Number Ranging from 1 to 2

Mizukaki, T.*

*The First Research Center, Technical Research and Development Institute, Japan Defense Agency, Naka-Meguro, Meguro, Tokyo, 153-8630, Japan.
(Current affiliation: Dept. of Aeronautics and Astronautics, School of Engineering, Tokai University, 1117, Kitakaname, Hiratsuka, Kanagawa, 259-1292 Japan.) E-mail: mizukaki@keyaki.cc.u-tokai.ac.jp

Received 26 December 2006
Revised 7 January 2008

Abstract : Using a ballistic range with a small single-stage powder gun, characteristics of detached shock waves around cylindrical projectiles were investigated. The detaches shock waves were analyzed quantitatively by visualization method. The projectiles were made of steel, with a diameter of 5.56 mm and with a mass of 1.77 g. The projectiles were ejected into the test section of the ballistic range at supersonic speeds. Direction-indicating color schlieren method (DInCS) was used to visualize the flow field. The stand-off distance of the detached shock waves and the shape were obtained as the function of Mach number. The functions were compared with the results obtained by wind tunnel experiments. Analyzed images provided the quantitative information on shock shapes. The results were as follows: (1) the stand-off distances of the detached shock waves have been shown as exponential functions of Mach number; (2) the shapes of the shock waves have been found as quadratic functions of Mach number. The differences in the functions between this paper and a wind tunnel test were shown.

Keywords : Flow visualization, High-speed projectiles, Detached shock waves.

1. Introduction

This paper describes preliminary results of the research investigating the flow fields around supersonic projectiles by free-flight experiments.

Flow visualization is a crucial technique for high-speed gasdynamics. Almost all the reports on experiments dealing with supersonic flow describe properties of flow field with flow visualization techniques. Schlieren and shadow photogram are the popular methods having been used for shock wave visualization since Ernst Mach succeeded in taking the photo of shock waves around a bullet at supersonic speed. Recently, various flow visualization techniques are used for the research of shock waves and high-speed flows (Desse et al., 2006; Mizukaki, 2007; Mizukaki, 2007; Ono et al., 2007). Analysis of the shape of visualized shock waves suggests flow structures and aerodynamic forces around an object at supersonic speed. For the design of supersonic aircrafts, therefore, both the shape and the location of attached/detached shock waves around fuselage and wings are critical information for safety and economical cursing. For examples, shapes and shock stand-off distances are required to calculate lift and drag force on nose and fuselage. Few data, however, have been reported on this topic, at speed around Mach unity. This knowledge will be required to develop a sonic cruiser and simulate re-entry of a space shuttle. Recently, the next generation of supersonic

transport has gained interest as an alternative to Concorde. The characteristics of the shock waves around projectiles will provide fundamental information contributing to the plane.

Heberle et al. (1950) reported the shapes of shock waves generated by spheres and cones at speeds between Mach 1.17 and 1.81 in a wind tunnel. Moeckel (1949) described the prediction method for the shapes and the locations of detached shock waves generated by slender bodies. The forms were in good agreement with results from wind tunnel experiments. Solomon (1954) compared the experimental results obtained with a transonic wind tunnel with those predicted by numerical method, on the flow fields around cone-cylinders and slender bodies. Laitone and Pardee (1947) have studied the supersonic flow fields around slender bodies at speeds of slightly above Mach unity. They have shown the relationship between the stand-off distance and the shape of projectiles as the function of Mach number. Kikuchi et al. (2005) have verified the stand-off distance of the detached shocks generated by spheres at speed of Mach unity using a single-stage gas gun.

The great majority of the work studying detached shock waves around cylindrical bodies has examined with wind tunnels. Several authors have developed theoretical prediction methods for the shapes of shock waves, but these theories based on the data which were obtained by wind tunnel experiments. For ordinary wind tunnel tests, the models to be examined must be fixed at a balance in test section and air is blown through the test section. On the other hand, for ballistic ranges, the models are accelerated to supersonic speed in-short-time toward free-space.

The purposes of the present paper are as follows: first, developing an small-size free-flight experimental facility with a small caliber single-stage powder gun, and evaluating its applicability for research on the flow field around high-speed projectiles; second, measuring the shape of the detached shock waves around cylindrical bodies flying between Mach unity and two, and finally, clarifying differences in the results between free-flight experiments and those by wind tunnel experiments.

2. Experimental Method

The dimensions of the projectile are shown in Fig. 1. The projectile was made of steel. Its mass was 1.77 ± 0.01 g and its shape was cylindrical with 5.46 mm diameter and 9.75 mm length. A schematic diagram of the experimental setup is shown in Fig. 2. A small caliber powder gun (SHS) with an acceleration tube with approximately 460 mm length and 5.56 mm inner diameter was installed to launch the projectiles. The firing signal from the trigger generator (TG) activated the solenoid coil (S) to tense the wire connected to the trigger of SHS. The velocity of the projectile at muzzle was varied by changing the loading position from the end of the chamber. This velocity was estimated by the laser-cutoff method. Semiconductor lasers (LD, wavelength: 780 nm, power: 4.5 mW, beam shape: 4.4 mm by 1.7 mm, ThorLabs CPS192) and photo sensors (PD, PIN-photodiode, rise-time: 1 ns, ThorLabs DET210) were used. Two pairs of LD-PD were set at 10 mm and 135 mm distance from the muzzle. The velocity was estimated from the time difference of light interruption between the first and the second pair. After detecting the signal indicating the firing, the digital phosphor oscilloscope (DPO, 1 GHz, 10 GSs, Tektronix TDS7104) generated a signal for triggering visualization apparatus. After being time delayed with the digital-retarder (DR, Sugawara RE-306), the signal activated the power source for visualization (PS) and initiated the spark head (SH). The shaded area in Fig. 2 indicates the visualized area.

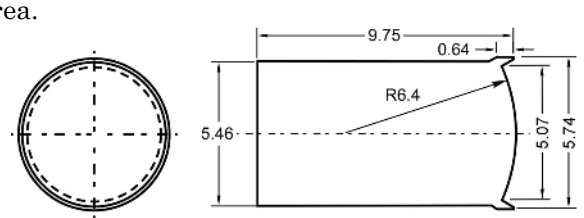

Fig. 1. Cylindrical model (unit: mm).

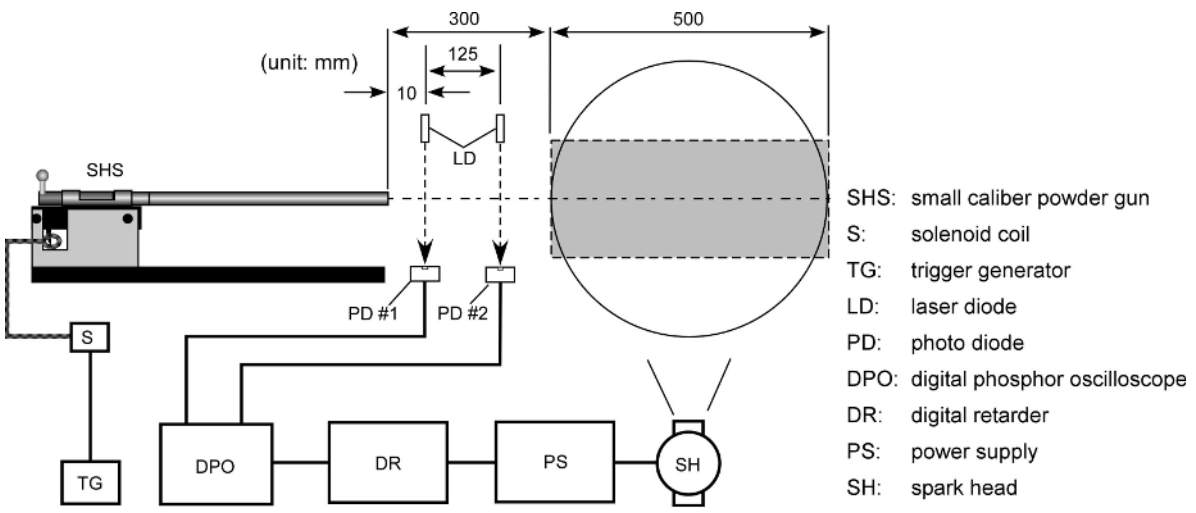

Fig. 2. Schematic diagram of experimental setup.

In the present paper, direction-indicating color schlieren method (DInCS) was employed to visualize the flow fields around projectile flying at Mach 2.0, 1.5, and 1.1. A schematic diagram of an optical alignment of DInCS is shown in Fig. 3. Generally, schlieren method provides monochrome images. The images indicate a one-dimensional density gradient of flow fields. In contrast, DInCS provides images indicating a two-dimensional density gradient by color. This technique is based on the proposal by Settles (1982). By using the color source mask shown in Fig. 4(a), the colors appearing in observed images indicate two-dimensional density gradient, as shown in Fig. 4(b). The inner diameter of the mask should not be smaller than about 6 mm because of diffraction effects, while the width of colored bands may vary from 0.25 mm to 1.5 mm. Narrow color bands cause an early overshooting while broad bands lead to a desideration of colors in observed images. DInCS, therefore, can measure structures of flow fields in detail. A high-intensity and short-duration Xe spark light (NanoSpark, NS-4000P, Biolek) was used as a light source. Visualized flow fields were recorded with a digital still camera with a 4024 × 1324 pixel resolution (Nikon D1x). Several literature describe DInCS in detail (Kleine et al., 1991; Settles, 2001; Mizukaki et al., 2004).

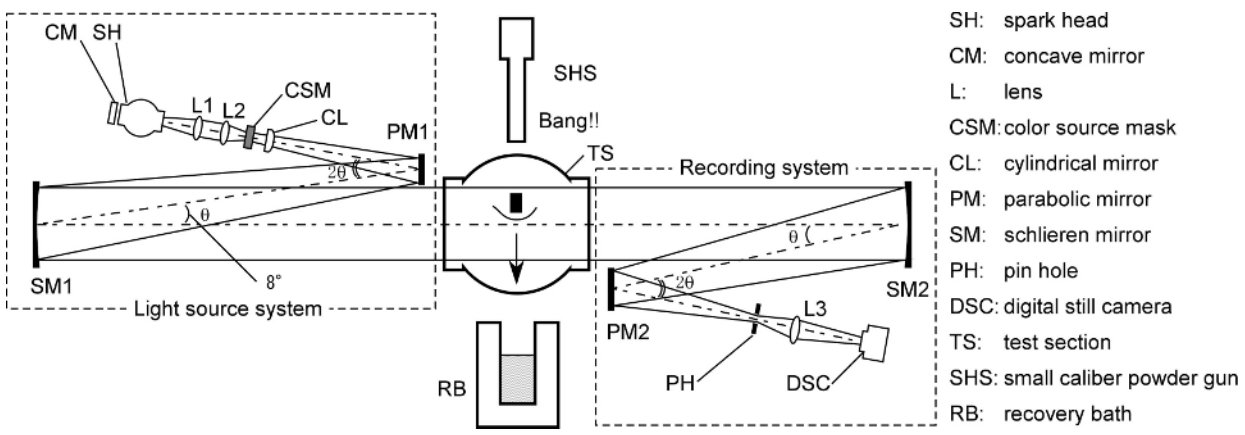

Fig. 3. Schematic diagram of optical visualization setup for DInCS.

The sensitivity of DInCS can easily be calibrated by inserting a reference with known refractive index into the test section. As already suggested by Schardin (1942), a plano-convex lens with a large focal length is a suitable reference. The reference causes the deflection of a center light beam of

$$\varepsilon \approx \tan\varepsilon = \frac{y_L}{f} \ , \tag{1}$$

where y_L is the distance from the line and f is the focal length of the reference lens. The deflection angle of the light beam for a tow-dimensional flow is denoted as

$$\varepsilon = \frac{L}{n}\left.\frac{\partial n}{\partial x}\right|_P \ , \tag{2}$$

where L is the width of the test section ($L = 0.3$ m for the present paper), n is the refractive index at a given point P and x is a coordinate which is perpendicular to the optical path. By the relation between the refractive index and the density:

$$n - 1 = K\rho \ , \tag{3}$$

with equations (1) and (2), the refractive index gradient is:

$$\left.\frac{\partial \rho}{\partial x}\right|_P = \frac{y_L}{LKf}(1 + K\rho) \approx \frac{y_L}{LKf} \ , \tag{4}$$

where ρ is the density at a given point P in the test section and K is the Gladstone-Dale constant of the test gas (0.23×10^{-3} m^3 kg^{-1}).

The reference lens used here had a focal length of 10 m and a diameter of 30 mm. For the one-dimensional method, equation (4) yields that one millimeter of y_L corresponds to the density gradient in air of roughly 1.45 kg m^{-4}, the maximum total gradient range covered by the lens being -21.7 kg m^{-4} to +21.7 kg m^{-4}.

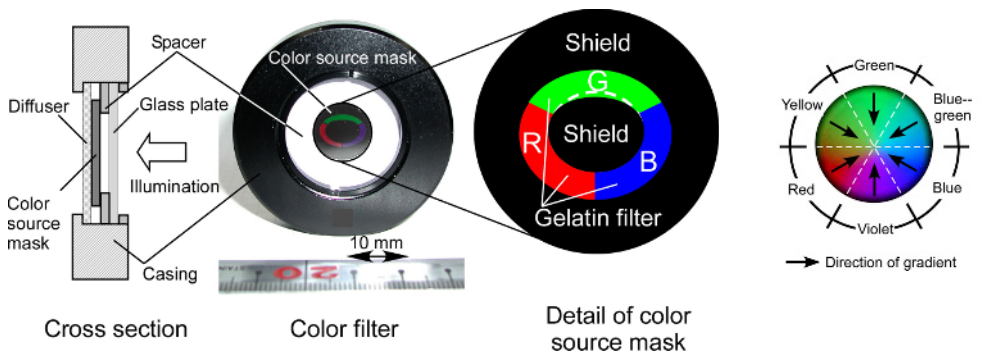

Fig. 4. Color source mask and reference image by long focal lens.

The spherical shock waves generated by the explosion of 10 mg Silver-azide in air are shown in Fig. 5. Figures 5(a) and (b) were recorded by ordinary schlieren method at 300 μs and at 150 μs by DInCS after ignition, respectively. One can recognize the color graduation showing the direction of density along the shock front SF in Fig. 5(b) while Fig. 5(a) only shows intensity gradient. Detail phenomena inside secondary shock wave SS can be clearly observed in Fig. 5(b).

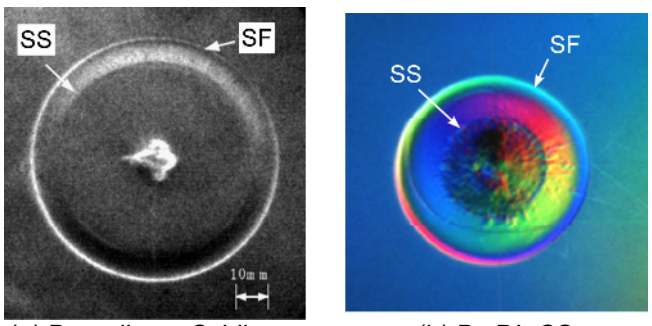

(a) By ordinary Schlieren (b) By DInCS

Fig. 5. Visualized spherical shock; SF: shock front, SS: secondary shock.

3. Results

Global flow fields (far field) around the projectiles at supersonic speeds are shown as time-resolution images in Fig. 6. Visualized images, numerically analyzed flow fields, and the sketches of the flow fields around the projectiles are shown in Fig. 7. Two-dimensional and axially-symmetric Euler equations were used for numerical analysis. The adaptive mesh method was employed to capture shock waves (Toro, 1989 and 1999).

Including detached shock waves, flow fields around the projectiles have been clearly visualized in Fig. 7. Shapes of the detached shock waves depend on both Mach number and the half-angle of apex of the projectile. Half-angle: 90 degrees, regularly provides detached shock waves. The curvature of the detached shock waves increased with increasing Mach number while the stand-off distance decreased. The flow coming along the symmetrical axis of the projectiles decreased its speed to subsonic after passing the shock front and to zero at the stagnation point. After passing the sonic line emanating from the front rim toward the shock front, the flow run along the side surface and was accelerated to supersonic speed again. The accelerated flow generated the shock waves SW1 from the side surface. At the rear fin of the projectile, oblique shock waves SW2 were developed. The angle of SW2 was higher than that of SW1 so that both the shock waves overlapped and propagated toward far field. The overlap was observed at all Mach numbers. Behind the projectile, tailing shock waves were observed because of interference of the supersonic flow with wake.

4. Discussion

On the detached shock waves observed here, we can approximate the shock stand-off distance ratio δ/d, and the shape as functions of the Mach number M, shown as Eq. (5) and Eq. (6), respectively (Heberle et al., 1950). Here, δ and d are the shock stand-off distance from the projectile to the shock front, and the diameter of the projectile, respectively. The shapes of the detached shock waves on visualized images were converted to coordinate data. The projectiles were assumed to fly along the y-axis toward the minus region. The x-axis crosses the y-axis at a right angle. The apex of the detached shock wave is at the origin. Using least squares approximation by Eq. (5) and Eq. (6), we determined the values of a, b, c_2, and c_4 for each experimental conditions. The calculated coefficients are shown in Table 1.

$$\frac{\delta}{d} = a \cdot (M-1)^b \tag{5}$$

$$y = c_2 \cdot x^2 + c_4 \cdot x^4 \text{, where } c_2 = 1 - e^{\alpha \cdot (M-1)},\ c_4 = \beta \cdot (M-1). \tag{6}$$

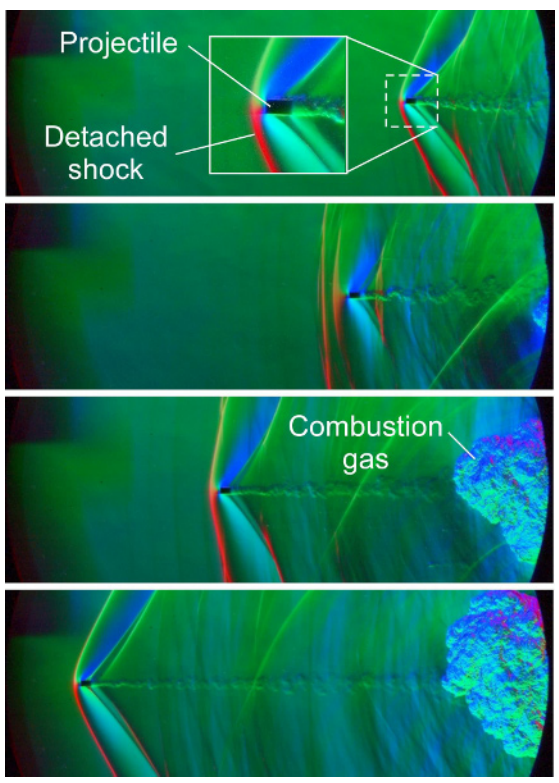

(a) M = 1.1

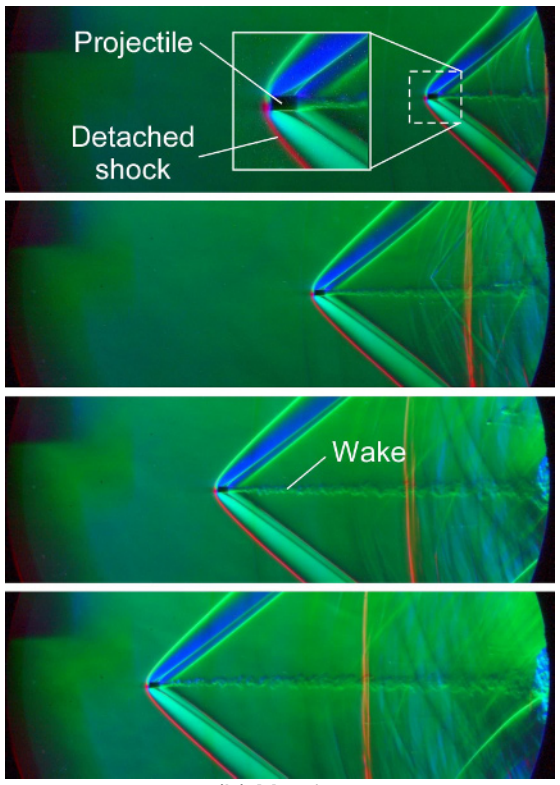

(b) M = 1.5

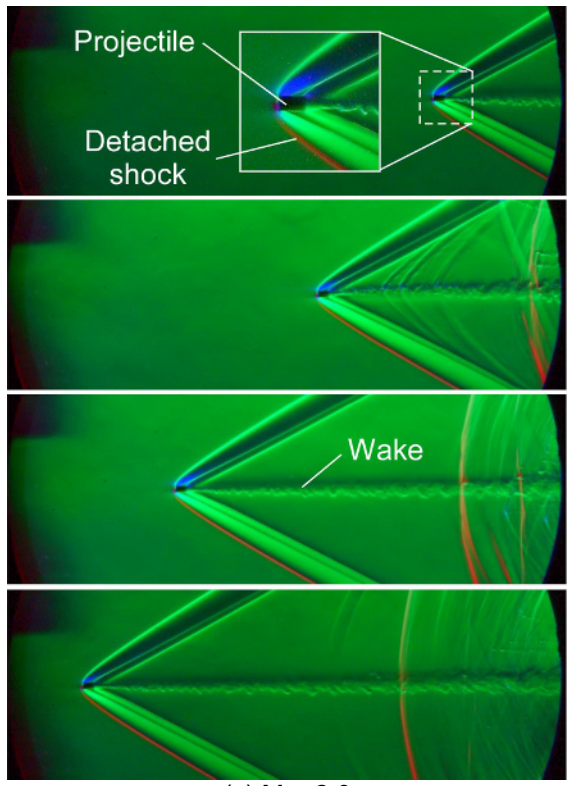

(c) M = 2.0

Fig. 6. Visualized flow fields at far fields of the cylindrical models; (a) M = 1.1, (b) M = 1.5, (c) M = 2.0, time interval: 250 μs.

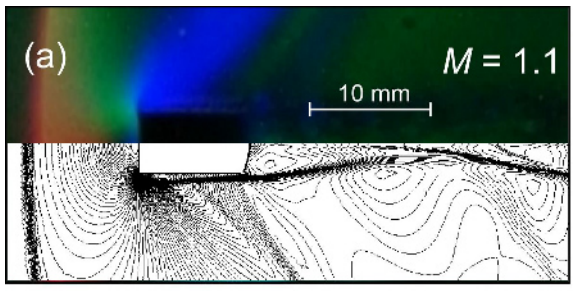

Visualized image and numerical analysis

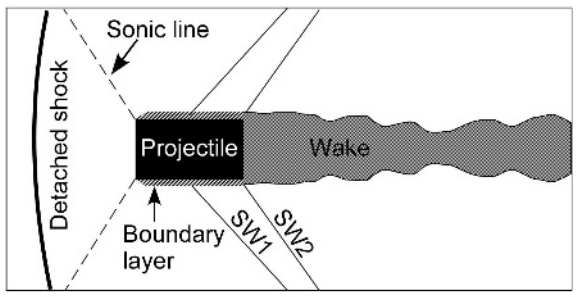

Sketch

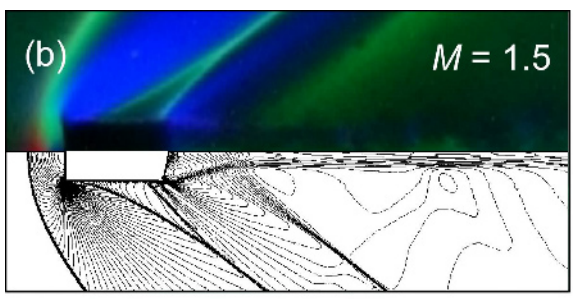

Visualized image and numerical analysis

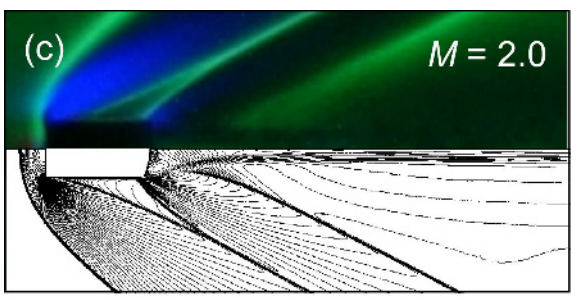

Visualized image and numerical analysis

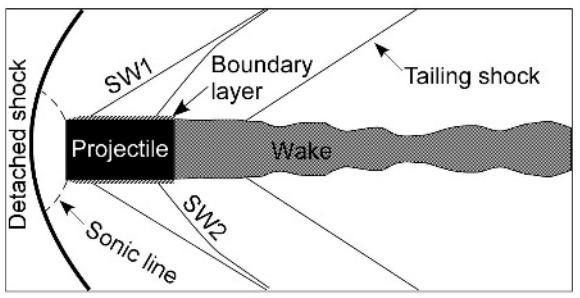

Sketch

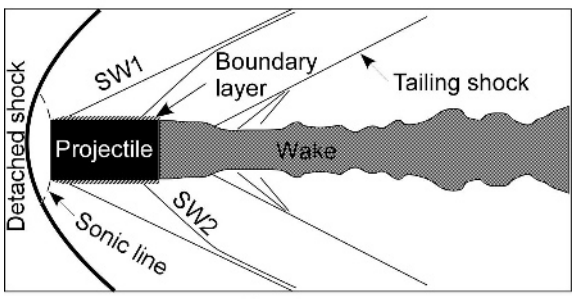

Sketch

Fig. 7. Flow fields near cylindrical projectiles; (a) M = 1.1, (b) M = 1.5, (c) M = 2.0, Numerical analysis is shown by density contours.

The relationship between M and δ/d is shown in Fig. 8. Circles indicate the present experiments (free-flight) and dashed line the data obtained by a wind tunnel test (Heberle et al., 1950). The shock stand-off distance indicated slightly different characteristics with those in the literature. It should be noted that, in the literature, the detached shock waves at slightly above Mach unity were not examined. Generally, at wind tunnel tests examining the flow around Mach unity, a precise control on flow velocity must be taken because fluctuations in Mach number drastically change the characteristic of the flow. There have been small numbers of reports on the visualization

of shock waves around the projectile at this velocity range. The coefficients a and b of the shock stand-off distances has differences between the present result (free-flight) and the literature (wind tunnel). The differences are approximately 10% for the coefficient a and 24% for the coefficient b. The coefficients of shape function (c_2 and c_4) are shown in Fig. 9. Circles and solid lines indicate the experimental results, and dashed lines show the fitted curves of the literature by Eq. (6).

Shock shape comparisons show results as follows: (1) the shape of the shock waves does not have a significant dependence on vertex semiangle up to 45 degrees, and is similar to that of a sphere; (2) At Mach 1.5, the difference of the shape coefficient c_2 between vertex semiangle 45/35 and 60 degrees is approximately one-thirds; (3) The coefficient c_2 at 90 degrees (cylinder) is approximately one-third that of 45/35 degrees or sphere.

In the present paper, the projectiles flew in room air. The Reynolds number here, therefore, was about 1.2×10^5 for the diameter of the cylinder as the characteristic length, while the Reynolds number of a typical transonic transporter at cruising speed is about 10^8. Both the shock shape and the shock stand-off distance obtained here would be analogous to those by a typical transonic transporter, although viscosity-related phenomena such as wake are not to them.

Table. 1. Geometric characteristics of detached shock waves.

	Stand-off distance		Shock shape		
	a	b	θ	α	β
The present experiment (Free-flight test)	0.43	– 0.62	90 (cylinder)	– 0.240	–0.001
Heberle et al. (1950) (Wind tunnel test)	0.48	– 0.50	60	– 0.448	– 0.012
			45	– 0.736	– 0.134
			35	– 0.742	– 0.052

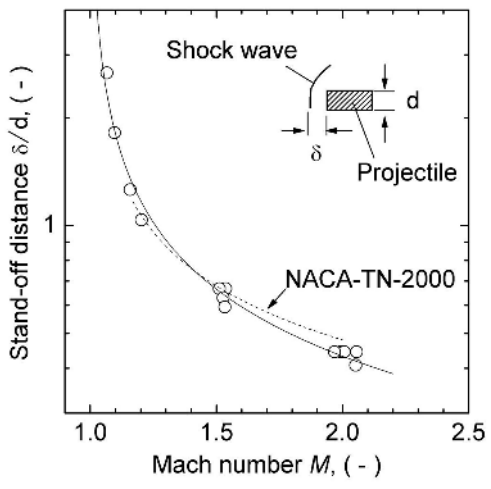

Fig. 8. Shock stand-off distance for cylinder.

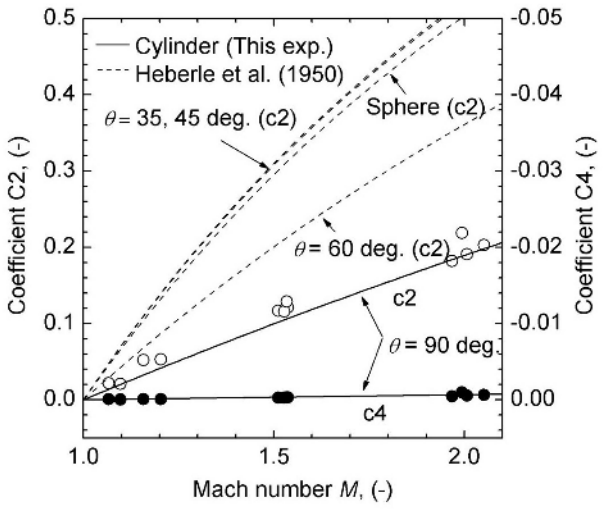

Fig. 9. Coefficients of the shock shape function.

5. Conclusions

The author developed a free-flight experimental facility with a small caliber single-stage powder gun. Using the facility, we have visualized the flow fields around cylindrical projectiles at speeds ranging from Mach unity to two. The shock stand-off distances have been indicated as functions of Mach

number. We can conclude the present study as follows:

(1) We demonstrated that free-flight experiments can easily provide the information on the shock waves around the projectile at speed in the vicinity of Mach unity;

(2) At the same flight Mach number, a cylindrical projectile has a smaller curvature than a spherical projectile. For example, at Mach 1.5, the second-order coefficient (C_2) of the quadratic function that indicates the shape of the detached shock wave for the cylindrical projectile has one-third of the value of the spherical projectile.

Acknowledgements

The author would like to thank Dr. Atsushi Abe of Itochu Techno-Solution Corp. for his helpful advice for the numerical analysis of the flow fields.

References

Desse, J. M. and Tribillon, J. L., State the Art of Color Interferometry at ONERA, Journal of Visualization, 9-4 (2006), 363-371.
Heberle, J. W., Wood, G. P. and Gooderum, P. B., Data on shape and location of detached shock waves on cones and spheres, NACA Technical Note, TN-2000, (1950).
Kikuchi, T., Numata, D., Ohtani, K., Kikuta, K., Ojima, H., Sun, M. and Takayama, K., Visualization of flow around a transonic free flight projectile, Proceedings of the 25th International Symposium on Shock Waves (Bangalore, India), (2005),
Kleine, H. and Grönig, H., Color schlieren methods in shock wave research, Shock Waves, 1 (1991), 51-63.
Laitone, E. V. and Pardee, O. O. M., Location of detached shock wave in front of a body moving at supersonic speeds, NACA Research Memorandum, RM-A7B10, (1947).
Mizukaki, T., Visualization and force measurement of high-temperature, supersonic impulse jet impinging on baffle plate, Journal of Visualization, 10-2 (2007), 227-235.
Mizukaki, T., Visualization of developing high temperature supersonic impulse jet induced by blast wave simulator, Journal of Visualization, 10-1 (2007), 91-98.
Mizukaki, T. and Arisawa, H., Visualization of gun muzzle blast wave using direction-indicating color schlieren method, Technical Report 6852, Technical Research and Development Institute, Japan Defense Agency, (2004).
Moeckel, W. E., Approximate method for predicting form and location of detached shock waves ahead of plane or axially symmetric bodies, NACA Technical Note, TN-1921, (1949).
Ono, N., Otomo, Y. and Koike, K., Behavior of underexpanded plasma jet in strong magnetic field, Journal of Visualization, 10-2 (2007), 237-244.
Schardin, H., Die Schlierenverfahren und ihre Anwendungen, Erg der exakt Naturwiss, 20 (1942), 303.
Settles, G. S., Color schlieren optics - A review of techniques and applications, Flow visualization II (ed. W. Merzkirch), (1982), Hemisphere Publishing Corp.
Settles, G. S., Schlieren and Shadowgraph Techniques, (2001), Springer-Verlag, Berlin.
Solomon, G. E., Transonic flow past cone cylinders, NACA Technical Note, TN-3213, (1954).
Toro, E. F., A weighted average flux method for hyperbolic conservation laws, Proc. R. Soc. Lond., A 423, (1989), 401-418.
Toro, E. F., Riemann solvers and numerical methods for fluid dynamics, (1999), Springer, Berlin Heidelberg.

Author Profile

Toshiharu Mizukaki: He received his B Sc (Sc) in Physics in 1991 from Tokyo University of Science. Form 1991 to 1999, he worked in Japan Atomic Energy Agency (JAEA) as a scientist. He received his Ph.D. in Aerospace Engineering in 2001 from Tohoku University. He worked in NASA Langley Research Center as a visiting scientist in 2001, in Technical Research and Development Institute of Japan Defense Agency from 2002 to 2005, and in Department of Aerospace Engineering, Indian Institute of Science in 2005. He has been working in Department of Aeronautics and Astronautics, School of Engineering, Tokai University, as an associate professor since 2006. His research interests are Shock Waves, High-Speed Launch System, Flow Visualization and Laser-applied measurement Techniques.